*ISSN 1392-1207. MECHANIKA. Vol. 30, No. 4, 2024: 333–340*

# Performance of Elastohydrodynamic Inclined Fixed Pad Thrust Bearing with Ultra Low Clearance

**Nahui WANG*, Yongbin ZHANG****
**College of Mechanical Engineering, Changzhou University, Changzhou, Jiangsu Province, China*
***College of Mechanical Engineering, Changzhou University, Changzhou, Jiangsu Province, China,*
*E-mail: engmech1@sina.com (Corresponding author)*
https://doi.org/10.5755/j02.mech.36547

## 1. Introduction

Hydrodynamic thrust bearings are one of the fundamental mechanical components for supporting the rotating shafts with the axial loads with the purpose of low friction and negligible surface wear. Classical hydrodynamic lubrication theories [1] have been developed well for these bearings based on the assumptions of the Newtonian fluid, the smooth bearing surfaces and the isothermal condition. In severe operating conditions with heavy loads and high sliding speeds, the effects of the fluid non-Newtonian shear thinning [2, 3], the surface roughness [4, 5], the fluid film viscous heating [6, 7] and the surface elastic deformation [8, 9] were also incorporated, since in such bearings the surface separations are comparable to both the surface roughness and the magnitudes of the surface elastic deformations and the film shear strain rates are high. Yan et al. [10] showed that the wall slippage effect can result in the greatly reduced surface clearance and even the film breakdown in a hydrodynamic step bearing for a given load. In the big-size hydrodynamic thrust bearings with heavy loads and high sliding speeds such as applied in hydrogenerators, the minimum surface clearances are very low and even vanishing owing to the thermoelastic deformation of the bearing surfaces [11-13]. On the other hand, the surface clearances in micro thrust bearings are intrinsically as low as on the 1nm or 10nm scales [14-16]. In these macro or micro thrust bearings with ultra-low clearances, the hydrodynamic status is actually more complicated than ever expected, and it is in the mixed lubrication where different lubrication regimes (physically adsorbed layer boundary lubrication and sandwich film lubrication) respectively occur in different irregular areas (owing to different surface separations) if the surface roughness is incorporated. The elastic deformations of the bearing surfaces surely significantly change the areas where the different films are distributed, as they are at least on the same scale with or even much greater than the bearing clearances. Conventional modeling of mixed lubrication in the thrust bearing omitted these complicated phenomena in the condition of much higher bearing clearances [17-20].

With the increase of the load or with the reduction of the sliding speed, the bearing clearance will be ultra-low and only on the 1nm scale. In this case, locally or even in the whole bearing the continuum fluid film can disappear and only the adsorbed layers on the bearing surfaces exist. This type of bearing may be in the new mode of mixed lubrication where different flow regimes occur respectively in different areas i.e. the pure adsorbed layer and the sandwich film simultaneously occur respectively in different lubricated areas. Surely, in such a bearing the effect of the surface elastic deformation should be significant as the magnitude of the surface elastic deformation is much comparable to or even much greater than the surface separation. Currently, the study is absent on this type of bearing.

The present paper aims to analytically investigate the performance of the hydrodynamic inclined fixed pad thrust bearing with ultra-low clearance by incorporating both the effects of the adsorbed layer and the surface elastic deformation. In the pure adsorbed layer area, the flow is described by the molecular-scale non-continuum flow equation; In the other area, the sandwich film flow is described by Zhang's multiscale flow equations [21]. The present study is more progressive than the research before in two regards i.e. by exploring the much smaller bearing clearance with the intermediate continuum fluid film locally vanishing and by considering the elastic deformations of the bearing surfaces. The mathematical equations have been derived respectively for calculating the hydrodynamic pressures and the carried load of the studied bearing. The numerical calculations were made for solving these equations. The obtained results reveal the important influences of both the adsorbed layer and the surface elastic deformation on the performance of this new mode of the bearing.

## 2. Elastohydrodynamic thrust bearing with ultra-low clearance

Fig. 1 shows the studied hydrodynamic inclined fixed pad thrust bearing with ultra-low clearance involving the effect of the surface elastic deformation. The bearing clearance is so low that in part of the lubricated area (in the outlet zone) the intermediate continuum fluid film is squeezed out and only the adsorbed layer exists, while in the other lubricated area the surface separations are big enough so that the continuum fluid film is contained between the two adsorbed layers. For a given operating condition, the surface elastic deformation results in the denting of the surface and the increase of the surface separation so that the area where the pure adsorbed layer exits is reduced and the sandwich film area is increased. The films in this bearing appear quite mixed with different rheologies. The previous analysis thus fails and the new analytical tool should be developed for this bearing.

In Fig. 1, $u$ is the sliding speed, $h_{bf}$ is the thickness of the physically adsorbed layer, $h$ is the thickness of the intermediate continuum fluid film, $h_{tot}$ is the surface separation, $h_{tot,o}$ is the surface separation on the exit of the bearing, $\theta$ is the tilting angle, and $l$ is the width of the bearing.

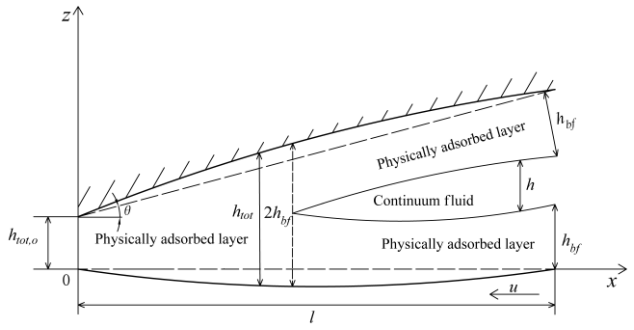


Fig. 1 The studied hydrodynamic inclined fixed pad thrust bearing with ultra-low clearance when the effect of the surface elastic deformation is involved

## 3. Mathematical analysis

In the pure adsorbed layer area, there are only several molecule layers adhering to the bearing surfaces, the rheological properties of which are largely influenced by the interaction between the fluid and the bearing surface. The flow in this area is essentially molecular-scale non-continuum and the rheological evolution such as the enhancement of both the effective viscosity and the average density of the adsorbed layer should be considered. Also the discontinuity and inhomogeneity across the adsorbed layer thickness should be incorporated. In these circumstances, the molecular-scale non-continuum flow equation is used to describe the flow in the pure adsorbed layer area. In the sandwich film area, the flow regimes of the adsorbed layer and the intermediate continuum fluid are radically different, and also there are the coupled effect between the adsorbed layer and the intermediate continuum fluid [21]. Zhang's multiscale flow equations are used to describe the flow in the sandwich film area.

For simplifying the problem and being focused on the issues, the present analysis is based on the assumptions of two identical adsorbed layers, negligible side leakage and film viscous heating, smooth bearing surfaces, and no interfacial slippage.

### 3.1. Core equations

According to Zhang's multiscale flow equations [21], in the sandwich film area the total mass flow rate per unit contact length through the bearing is:

$$q_m = \rho_{bf,1}^{eff}\left[\frac{F_1 h_{bf}^3}{6\eta_{bf,1}^{eff}}\frac{dp}{dx} - \frac{h_{bf}^3}{\eta_{bf,1}^{eff}}\frac{dp}{dx}\left(1+\frac{1}{2\lambda_{bf}} - \frac{q_0 - q_0^n}{q_0^{n-1} - q_0^n}\frac{\Delta_{n-2}}{h_{bf}}\right)\frac{\varepsilon}{1+\frac{\Delta x}{D}} - uh_{bf}\right] - \\ -\rho\left\{\frac{u}{2}h + \frac{h^3}{12\eta}\frac{dp}{dx} - \frac{h^3}{\eta_{bf,1}^{eff}}\frac{dp}{dx}\left[\frac{F_2\lambda_{bf}^2}{6} - \frac{\lambda_{bf}}{1+\frac{\Delta x}{D}}\left(\frac{1}{2}+\lambda_{bf} - \lambda_{bf}\frac{q_0 - q_0^n}{q_0^{n-1} - q_0^n}\frac{\Delta_{n-2}}{h_{bf}}\right)\right]\right\}, \quad (1)$$

where $\lambda_{bf} = h_{bf} / h$, $p$ is the film pressure, $x$ is the coordinate shown in Fig. 1, $\rho$ and $\eta$ are respectively the bulk density and the bulk viscosity of the fluid, $\rho_{bf,1}^{eff}$ and $\eta_{bf,1}^{eff}$ are respectively the average density and the effective viscosity of the adsorbed layer, $D$ is the fluid molecule diameter, $\Delta x$ is the separation between the neighboring fluid molecules in the $x$ coordinate direction in the adsorbed layer, $q_0$ is the average value of $\Delta_{j+1} / \Delta_j$ ($\Delta_j$ is the separation between the ($j$+1)-th and $j$-th fluid molecules across the adsorbed layer thickness), $n$ is the equivalent number of the fluid molecules across the adsorbed layer thickness, $\Delta_{n-2}$ is the separation between the neighboring fluid molecules across the adsorbed layer thickness just on the boundary between the adsorbed layer and the continuum fluid film, and the formulations of $F_1$, $F_2$, and $\varepsilon$ have been shown in [21].

In the pure adsorbed layer area, the total mass flow rate per unit contact length through the bearing is [21]:

$$q_m = \frac{S\rho_{bf,2}^{eff}h_{tot}^3}{12\eta_{bf,2}^{eff}}\frac{dp}{dx} - \frac{u}{2}h_{tot}\rho_{bf,2}^{eff}, \quad (2)$$

where $\rho_{bf,2}^{eff}$ and $\eta_{bf,2}^{eff}$ are respectively the average density and the effective viscosity of the adsorbed layer across the whole surface separation, and $S$ is the parameter accounting for the discontinuity and inhomogeneity effect of the adsorbed layer.

### 3.2. Numerical analysis

#### 3.2.1. Numerical calculation for film pressure and load

The incorporation of the surface elastic deformation causes the high non-linearity of the present problem. The numerical calculation is thus mandatory for finding the film pressure and load of the bearing. In the numerical analysis, there are evenly distributed ($N$+1) discretized points in the whole lubricated area in the present bearing.

By forward difference, the pressure gradient on the $i$-th discretized point is expressed as:

$$\left.\frac{dp}{dx}\right|_i = \frac{p_i - p_{i-1}}{\delta_x} = \begin{cases}\dfrac{a_i h_i + d_i}{c_i h_i^3 + b_i}, & \text{for } h_i > 0 \\ \dfrac{A_i}{h_{tot,i}^2} + \dfrac{B_i q_m}{h_{tot,i}^3}, & \text{for } h_{tot,i} \le 2h_{bf}\end{cases}, \quad (3)$$

where the formulations of, $a$, $b$, $c$, $d$, $A$ and $B$ have been shown in [21], the subscript "$i$" denotes the values on the $i$-th discretized point, and $\delta_x = l / N$.

By considering the surface elastic deformation, the surface separation on the $i$-th discretized point is expressed as:

$$h_{tot,i} = h_{oo} + x_i\tan\theta - \frac{2}{\pi E_v}\int_0^l p(s)\ln(x_i - s)^2\, ds, \quad (4)$$

here $h_{oo}$ is constant, $E_v$ is the compound Young's modulus of elasticity of two bearing surfaces, and $s$ is an integral variable.

The thickness of the intermediate continuum fluid film on the $i$-th discretized point is:

$$h_i = h_{tot,i} - 2h_{bf} . \quad (5)$$

Based on the boundary condition $p_0 = 0$, the pressure on each discretized point was calculated from the following equation:

$$p_i = \sum_{k=1}^{i} \left( p_k - p_{k-1} \right), \text{ for } i = 1, 2, \ldots, N , \quad (6)$$

where $(p_k - p_{k\text{-}1})$ is calculated from Eq. (3).

The load per unit contact length carried by the bearing is:

$$w = \delta_x \sum_{i=1}^{N-1} p_i . \quad (7)$$

3.2.2. Numerical integration for the surface elastic deformation and numerical solution procedure

The equation for the surface elastic deformation shows the following integral term:

$$\Theta_i = -\frac{2}{\pi E_v} \int_0^l p(s) \ln\left( x_i - s \right)^2 ds . \quad (8)$$

The exact calculation of Eq. (8) is impossible because of the unknown film pressure distribution. The numerical integration of Eq. (8) has been shown in [22]. The detailed numerical solution procedure is also shown in [22].

## 4. Formulation for fundamental parameters

The bulk density and bulk viscosity of the fluid on the $i$-th discretized point are respectively formulated as: $\rho_i = \rho_a(1+\beta \cdot p_{i\text{-}1})$, and $\eta_i = \eta_a \exp\left\{ (\ln \eta_a + 9.67)\left[ (1 + p_{i-1} \cdot 5.1\text{E}-9)^z - 1 \right] \right\}$ where $z = \alpha / \left[ (5.1E-9)\left( ln\,\eta_a + 9.67 \right) \right]$, $\rho_a$ and $\eta_a$ are respectively the bulk density and bulk viscosity of the fluid at ambient pressure; $\alpha$ and $\beta$ are respectively constant. In the sandwich film area, the average density and effective viscosity of the adsorbed layer across the adsorbed layer thickness on the $i$-th discretized point are respectively formulated as $\rho_{bf,1,i}^{eff} = C_{q1}(H_{bf,1})\rho_i$ and $\eta_{bf,1,i}^{eff} = C_{y1}(H_{bf,1})\eta_i$, where $C_{q1}$ and $C_{y1}$ are respectively the coefficients dependent on the adsorbed layer thickness, $H_{bf,1} = h_{bf} / h_{cr,bf,1}$, and $h_{cr,bf,1}$ is the critical thickness for characterizing the rheological properties of the adsorbed layers in the sandwich film area. In the pure adsorbed layer area, the average density and effective viscosity of the adsorbed layer across the whole surface separation on the $i$-th discretized point are respectively formulated as $\rho_{bf,2,i}^{eff} = C_{q2}(H_{bf,2})\rho_i$ and $\eta_{bf,2,i}^{eff} = C_{y2}(H_{bf,2})\eta_i$, where $C_{q2}$ and $C_{y2}$ are respectively the coefficients dependent on the surface separation, $H_{bf,2} = h_{tot} / h_{cr,bf,2}$ and $h_{cr,bf,2}$ is the critical thickness for characterizing the rheological properties of the adsorbed layers in the pure adsorbed layer area. The general form ($C_q(H_{bf})$) of $C_{q1}$ and $C_{q1}$ have been shown in [21]. The general form ($C_y(H_{bf})$) of $C_{y1}$ and $C_{y1}$ as well as the function $S(H_{bf,2})$ have also been shown in [21].

In all the calculations, the following parameter values were chosen: $D = 0.5$ nm, $N = 1000$, $\Delta_{n-2} / D = \Delta x / D = 0.15$, $l = 200$ μm, $\theta = (1\text{E}-4)$ rad, $\eta_a = 0.03$ Pa·s, $\alpha = (1.6\text{E}-8)$ m$^2$/N, $\beta = (4\text{E}-10)$ Pa$^{-1}$, $\vartheta = 0.2$.

Most of the characteristic parameter values respectively for the weak, medium and strong fluid-bearing surface interactions have been shown in [21]. Some of them are shown in Table 1. Different bearing surface materials were used. The corresponding values of $E_v$ for these materials are shown in Table 2. It is assumed that $\eta_{line,j} / \eta_{line,j+1} = q_0^{\gamma}$, where $\gamma$ is constant and $\eta_{line,j\text{-}1}$ is the local viscosity between the $j$-th and ($j$-1)-th fluid molecules across the adsorbed layer thickness.

Table 1

Values of $n$, $q_0$, $\gamma$, $h_{cr,bf,1}$ and $h_{cr,bf,2}$

| Parameter / Interaction | $n$ | $q_0$ | $\gamma$ | $h_{cr,bf,1}$, nm | $h_{cr,bf,2}$, nm |
|---|---|---|---|---|---|
| Strong | 8 | 1.2 | 1.5 | 40 | 80 |
| Medium | 5 | 1.1 | 1 | 20 | 40 |
| Weak | 3 | 1.03 | 0.5 | 7 | 14 |

Table 2

Compound Young's modulus of elasticity of different bearing surface materials

| Material | non crystalline silica | bronze | silicon | steel | silicon carbonized |
|---|---|---|---|---|---|
| $E_v$, GPa | 75 | 120 | 192 | 209 | 480 |

## 5. Results

5.1. Film pressure distributions

Fig. 2, a-c shows the influences of the surface elastic deformation on the film pressure distributions when the fluid-bearing surface interactions are respectively weak, medium and strong under different loads and the bearing surface is made of steel. Why the different loads were used for different fluid-bearing surface interactions is to obtain the hydrodynamic status shown in Fig. 1 where the sandwich film area and the pure adsorbed layer area coexist. It is shown that the surface elastic deformation significantly reduces the maximum film pressure and modifies the film pressure profile especially when the load is heavier and thus the magnitude of the surface elastic deformation is greater. This is particularly the case for the strong fluid-bearing surface interaction.

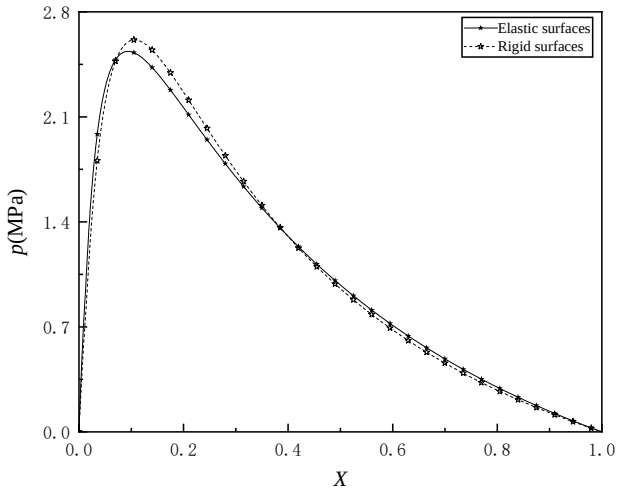


a

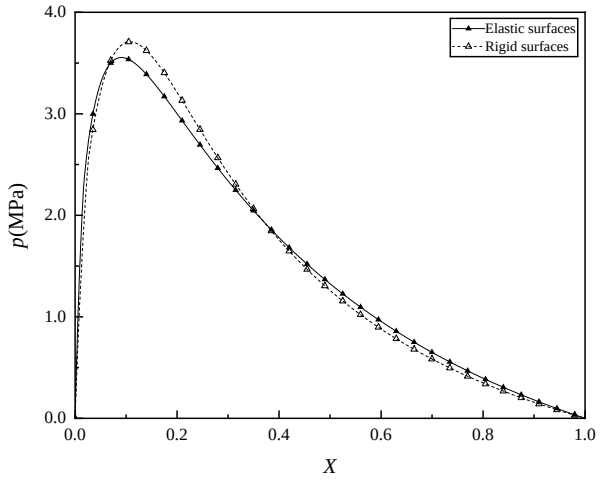


b

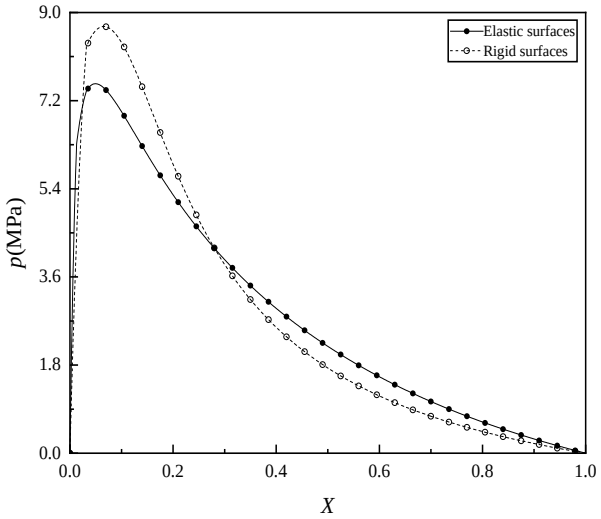


c

Fig. 2 Film pressure distributions in the bearing for different fluid-bearing surface interactions respectively for elastic and rigid surfaces when $u$ = 2.0E–5 m/s and the bearing surface is made of steel: a – for the weak interaction, $w$ = 220 N/m; b – for the medium interaction, $w$ = 306 N/m; c – for the strong interaction, $w$ = 562 N/m

Fig. 3 shows the influences of different bearing surface materials on the film pressure distribution in the bearing for the given load and sliding speed when the effect of the surface elastic deformation is considered. For the same operating conditions, these four different materials give different maximum film pressures and different film pressure profiles owing to their different Young's modulus of elasticity, which results in different magnitudes of the surface elastic deformation. Greater the Young's modulus of elasticity of the bearing surface material, steeper the film pressure distribution. This effect should be more significant when the load is heavier.

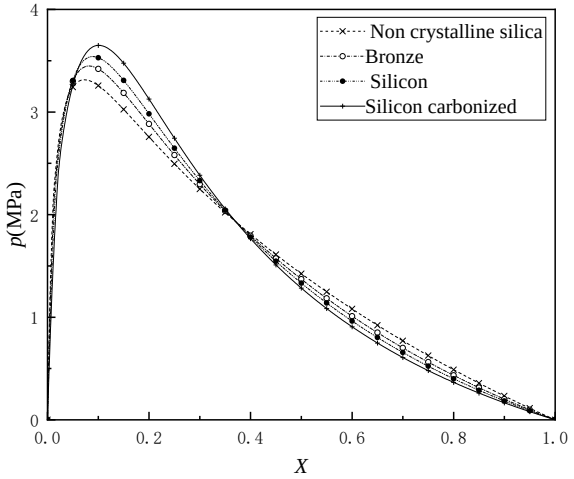


Fig. 3 Film pressure distributions in the bearing with different surface materials involving the surface elastic deformation for the medium fluid-bearing surface interaction when $u$ = 2.0E–5 m/s and $w$ = 306 N/m

5.2. Surface separation profile

Fig. 4, a-c shows the corresponding surface separation profiles involving the surface elastic deformation when the operating conditions are respectively the same as shown in Fig. 2, a-c. The surface elastic deformation significantly modifies the surface separation profile, reduces the surface separation in the inlet zone, but increases the surface separation in most of the outlet zone (except on the exit of the bearing), especially when the load is heavier. Although the pressures in the bearing are normal and no more than 10 MPa as shown in Fig. 2, a-c, the changes of the surface separations by the surface elastic deformation are on the same scale with the original bearing clearance, and their effects on the film pressures and load-carrying capacity of the bearing should undoubtedly be pronounced.

Fig. 5 shows the corresponding surface separation profiles for different bearing surface materials when the effect of the surface elastic deformation is considered and the film pressures are shown as in Fig. 3. For a given operating condition, the surface material has a strong influence on the surface separation profile in the bearing. For silicon carbonized, which has the highest Young's modulus of elasticity ( $E_v$ = 4.8E11 Pa ), the bearing surfaces are nearly rigid under the load; In this case, the calculation can ignore the effect of the surface elastic deformation. However, for non crystalline silica, which has the lowest Young's modulus of elasticity ( $E_v$ = 7.5E10 Pa ), the surface elastic deformation is very significant and it largely

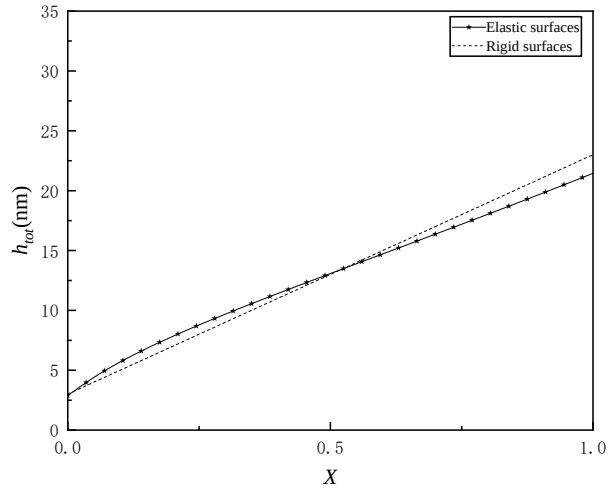


a

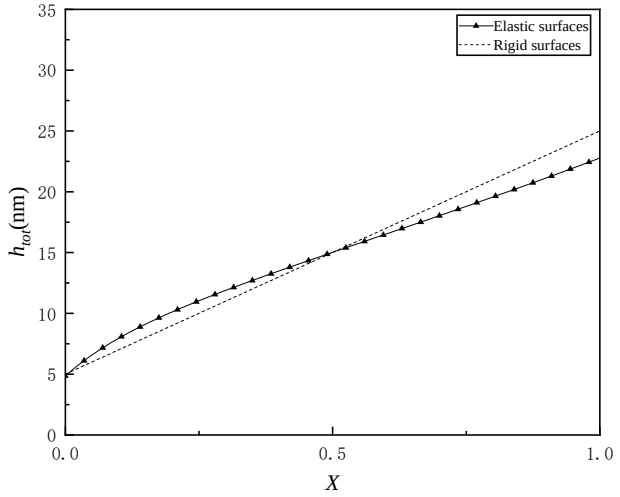


b

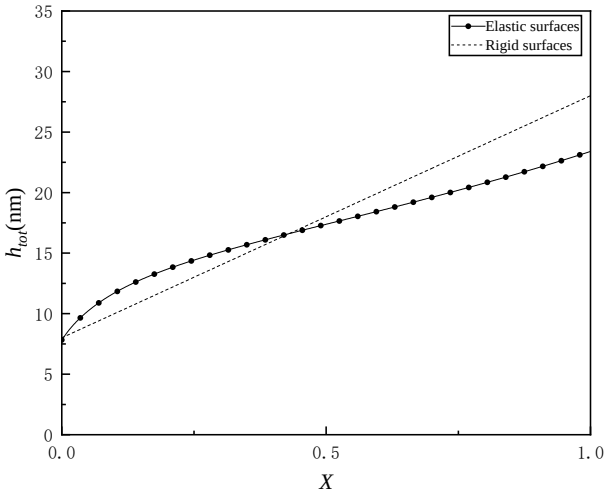


c

Fig. 4 Surface separation in the bearing for different fluid-bearing surface interactions considering elastic deformation when $u$ = 2.0E–5 m/s and the bearing surface is made of steel: a – for the weak interaction, $w$ = 220 N/m; b – for the medium interaction, $w$ = 306 N/m; c – for the strong interaction, $w$ = 562 N/m

modifies the surface separation profile. For a given bearing surface material, the influence of the surface elastic deformation on the bearing performance should obviously depend on the load.

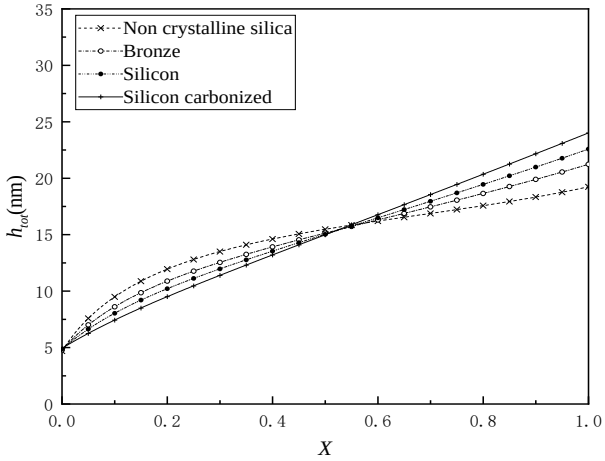


Fig. 5 Surface separation profiles of the bearing for different surface materials for the medium fluid-bearing surface interaction involving the surface elastic deformation when $u$ = 2.0E–5 m/s and $w$ = 306 N/m

5.3. Film stiffness and load-carrying capacity of the bearing

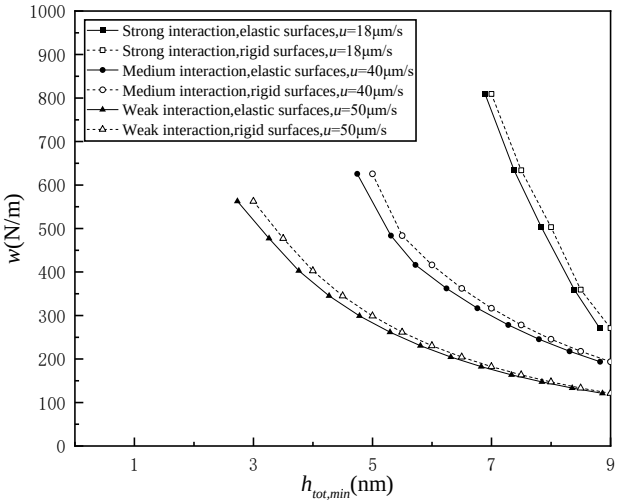


Fig. 6 Variations of the carried load of the bearing with the minimum surface separation $h_{tot,min}$ respectively for elastic and rigid bearing surfaces for different fluid-bearing surface interactions when the bearing surface is made of steel

Fig. 6 compares the load ($w$) versus minimum surface separation ($h_{tot,min}$) curves respectively for elastic and rigid surfaces when the sliding speed is given, the fluid-bearing surface interaction is respectively weak, medium and strong, and the bearing surface is made of steel. $h_{tot,min}$ is located on the exit of the bearing, and the slope of the curve is the film stiffness in the bearing. It is shown that the surface elastic deformation results in the reduced film stiffness.

Fig. 7 shows that for a given operating condition, when the bearing surface material is different, the film stiffness is different; The surface material with a higher

Young's modulus of elasticity gives a higher film stiffness. For the same value of $h_{tot,min}$ the carried load of the bearing is greater for the less elastic surface material, or for the same load the value of $h_{tot,min}$ is greater. This shows that the surface material influences the load-carrying capacity of the bearing owing to the surface elastic deformation.

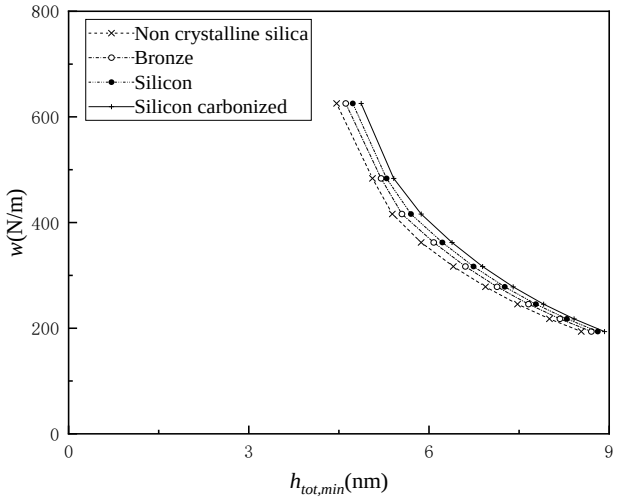


Fig. 7 Variations of the carried load of the bearing with the minimum surface separation $h_{tot,min}$ for different bearing surface materials for $u$ = 4.0E−5 m/s when the surface elastic deformation is involved

5.4. Variation of the load of the bearing with the sliding speed

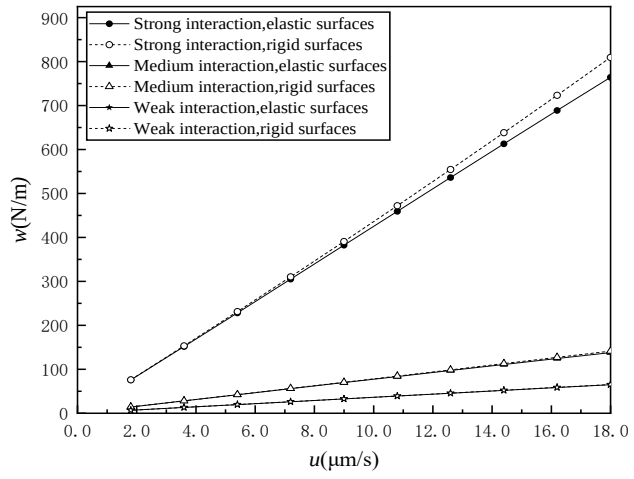


Fig. 8 Variations of the load of the bearing with the sliding speed respectively for elastic and rigid surfaces for different fluid-bearing surface interactions when $h_{tot,min}$ = 7 nm and the bearing surface is made of steel

Fig. 8 shows that whenever the bearing surface is rigid or in the elastic deformation, the carried load by the bearing is linearly increased with the increase of the sliding speed. However, the surface elastic deformation results in the reduced proportionality of the load with the sliding speed especially for the strong fluid-bearing surface interaction, which yields the highest film pressures and thus the greatest surface elastic deformation when the sliding speed is given. For the weak and medium fluid-bearing surface interactions, the two curves are nearly overlaid owing to the low film pressures and the resulting negligible effect of the surface elastic deformation.

## 6. Conclusions

The effect of the surface elastic deformation is analytically investigated in the hydrodynamic inclined fixed pad thrust bearing with ultra-low clearance. The hydrodynamic status in this bearing is mixed and it consists of the molecular-scale non-continuum hydrodynamics of the pure adsorbed layer and the hydrodynamics of the sandwich film which contains both the adsorbed layer and the intermediate continuum fluid film across the surface separation. The analysis should solve these two different flow regimes. Here, the molecular-scale non-continuum flow equation is used to describe the pure adsorbed layer flow, and Zhang's closed-form explicit multiscale flow equations are used to describe the sandwich film flow. Owing to the high non-linearity of the problem caused by the surface elastic deformation, the numerical calculations were carried out for finding the film pressures and carried load of the bearing. Different fluid-bearing surface interactions and different bearing surface materials were considered.

Based on the calculation results, the conclusions are drawn as follows:

The surface elastic deformation has a significant influence on the performance of the bearing. For a given load, it reduces the maximum film pressure and the minimum surface separation, and modifies both the film pressure profile and the surface separation profile.

The effect of the surface elastic deformation strongly depends on the fluid-bearing surface interaction. For a given operating condition, stronger the fluid-bearing surface interaction, more significant the effect of the surface elastic deformation.

The surface elastic deformation results in the reduced film stiffness in the bearing. The bearing surface material significantly influences the performance of the bearing. The less elastic surface material gives the higher film stiffness and the greater load-carrying capacity of the bearing.

Whenever the bearing surface is rigid or in the elastic deformation, the carried load of the bearing is linearly increased with the sliding speed. However, the surface elastic deformation results in the reduced proportionality of the bearing load with the sliding speed.

The effect of the surface elastic deformation heavily depends on the carried load of the bearing, which determines the magnitude of the surface elastic deformation. Whenever the film pressures are normal or very high in the bearing with ultra-low clearance, the effect of the surface elastic deformation should be involved when analyzing the bearing performance.

## References

1 **Pinkus, O.; Sternlicht, B.** 1961. Theory of hydrodynamic lubrication. New York: McGraw-Hill. 465p.

2 **Yadav, S. K.; Sharma, S. C.** 2016. Performance of hydrostatic textured thrust bearing with supply holes operating with non-Newtonian lubricant, Tribology

Transactions 59(3): 408-420.
https://doi.org/10.1080/10402004.2015.1083065.

3 **Kumar, V.; Shah, V. A.; Narwat, K.; Sharma, S. C.** 2022. Squeeze film operation of thrust bearing operating with shear-thinning lubricants, in: K. Govindan, H. Kumar, S. Yadav (Eds) Advances in Mechanical and Materials Technology, EMSME 2020 Lecture Notes in Mechanical Engineering, Springer, Singapore.
https://doi.org/10.1007/978-981-16-2794-1_9.

4 **Singh, U. P.** 2020. Mathematical Analysis of Effects of Surface Roughness on Steady Performance of Hydrostatic Thrust Bearings Lubricated with Rabinowitsch Type Fluids, Journal of Applied Fluid Mechanics 13(4): 1339-1347.
https://doi.org/10.36884/jafm.13.04.30682.

5 **Kumar, R.; Gopaliya, M. K.; Khan, H.; Azam, M. S.; Biswal, D. K.** 2023. Analysis of thrust pad bearing under mixed-EHL regime considering combined effect of deterministic and stochastic surface roughness, Journal of the Brazilian Society of Mechanical Science and Engineering 45: 559.
https://doi.org/10.1007/s40430-023-04464-8.

6 **Huebner, K. H.** 1974. A three-dimensional thermohydrodynamic analysis of sector thrust bearings, Tribology Transactions 17: 62-73.
https://doi.org/10.1080/05698197408981439.

7 **Tieu, A. K.** 1975. Numerical Simulation of Finite-Width Thrust Bearings, Taking into Account Viscosity Variation with Temperature and Pressure, Journal of Mechanical Engineering Science.17(1): 1-10.
https://doi.org/10.1243/JMES_JOUR_1975_017_003_02.

8 **Greenwood, J. A.; Wu, J. J.** 1995. Elasto-hydrodynamic lubrication of centrally pivoted thrust bearings, Journal of Physics D: Applied Physics 28(11): 2371-2377.
https://doi.org/10.1088/0022-3727/28/11/023.

9 **Brockett, T. S.; Barrett, L. E.; Allaire, P. E.** 1996. Thermoelastohydrodynamic Analysis of Fixed Geometry Thrust Bearings Including Runner Deformation, Tribology Transactions 39(3): 555–562.
https://doi.org/10.1080/10402009608983566.

10 **Yan, J.; Jiang, X.; Zhu, Y.; Zhang, Y. B.** 2014. An analysis for a limiting shear stress effect in a hydrodynamic step bearing. Part I. First mode of boundary slippage for film breakdown, Journal of the Balkan Tribological Association 20(2): 259-270.

11 **Ettles, C. M.** 1980. Size effects in tilting pad thrust bearings, Wear 59(1): 231-245.
https://doi.org/10.1016/0043-1648(80)90281-1.

12 **Kawaike, K.; Okano, K.; Furukawa, Y.** 1979. Performance of a large thrust bearing with minimized thermal distortion, Tribology Transactions 22: 125-134.
https://doi.org/10.1080/05698197908982908.

13 **Yuan, J. H.; Medley, J. B.; Ferguson, J. H.** 2001. Spring-Supported Thrust Bearings Used in Hydroelectric Generators: Comparison of Experimental Data with Numerical Predictions, Tribology Transactions 44(1): 27–34.
https://doi.org/10.1080/10402000108982422.

14 **Ho, C. M.; Tai, Y. C.** 1998. Micro-electro-mechanical-systems (MEMS) and fluid flows, Annual Review of Fluid Mechanics 30: 579-612.
https://doi.org/10.1146/ANNUREV.FLUID.30.1.579.

15 **Judy, J. W.** 2001. Microelectromechanical systems (MEMS): fabrication, design and applications, Smart Materials and Structures 10: 1115-1134.
https://doi.org/10.1088/0964-1726/10/6/301.

16 **Wong, C. W.; Zhang, X.; Jacobson, S. A.; Epstein, A. H.** 2004. A self-acting gas thrust bearing for high-speed microrotors, Journal of Microelectromechanical Systems 13(2): 158-164.
https://doi.org/10.1109/JMEMS.2004.824900.

17 **Zhang, X. H.; Xu, Y.; Jackson**, **R. L.** 2020, A mixed lubrication analysis of a thrust bearing with fractal rough surfaces, Proceedings of the Institution of Mechanical Engineers, Part J: Journal of Engineering Tribology 234(4): 608-621.
http://dx.doi.org/10.1177/1350650119867242.

18 **Zhang, X. H.; Jackson, R. L.** 2021. A mixed lubrication analysis of a flat-land thrust bearing with a surface optimisation method, Lubrication Science 33(6): 335-346.
https://doi.org/10.1002/ls.1556.

19 **Winkler, A.; Marian, M.; Tremmel, S.; Wartzack, S.** 2020. Numerical modeling of wear in a thrust roller bearing under mixed elastohydrodynamic lubrication, Lubricants 8(5): 58.
https://doi.org/10.3390/lubricants8050058.

20 **Jackson, R. L.; Green, I.** 2006. The behavior of thrust washer bearings considering mixed lubrication and asperity contact, Tribology Transactions 49: 233-247.
http://dx.doi.org/10.1080/05698190600614841.

21 **Wang, C.; Zhang, Y. B.** 2023. Surface roughness effect in hydrodynamic thrust bearing with ultra low clearance, International Journal for Engineering Modelling 36: 61-74.
https://hrcak.srce.hr/309811.

22 **Zhu, J. X.; Zhang, Y. B.** 2023. Effect of surface elastic deformation in hydrodynamic inclined fixed pad thrust bearing with low clearance, Mechanika 29(6): 454-461.
https://doi.org/10.5755/j02.mech.33803.

N. Wang, Y. Zhang

PERFORMANCE OF ELASTOHYDRODYNAMIC INCLINED FIXED PAD THRUST BEARING WITH ULTRA LOW CLEARANCE

S u m m a r y

This study investigates the performance of elastohydrodynamic inclined fixed pad thrust bearing with ultra-low clearance. The analysis was conducted using a multiscale approach by considering the surface elastic deformation, the physical adsorption layer and the fluid piezoviscous effect. Numerical calculations reveal that in this bearing the magnitude of the surface elastic deformation is comparable to both the surface separation and the adsorption layer thickness. Compared to the case of rigid bearing surfaces, the surface elastic deformation results in a significant reduction of the maximum hydrodynamic pressure in the bearing. For a given speed and load, when the fluid-bearing surface interaction is stronger, the influence of the surface elastic deformation on the bearing pressure is more significant. For different surface materials with quite different Young's modulus of elasticity, when the load and speed are given, the distributions of the film pressure and the surface separation in the bearing are obviously different. For a given load, the surface elastic deformation results in the reduction of the minimum surface separation. For a given minimum surface separation, the increase of the load with the sliding speed is more rapid for rigid bearing surfaces than for elastic bearing surfaces.

**Keywords**: adsorbed layer, elastohydrodynamics, multiscale, pressure load, thrust bearing.

Received March 5, 2024
Accepted August 19, 2024